

Numerical Analysis of the effect of Upstream Obstacles on Aerodynamic Performance of NACA 65-421 Airfoil Using RNG k-ε Model

Omar Badran¹, Ismail Masalha¹, Ali Alahmer^{2,*}, Zeeshan Azad³, Muhammad Virk³, Saad Ragab⁴, Kareem Akhtar⁵

¹Al-Balqa Applied University, Faculty of Engineering Technology, Amman – Jordan

²Department of Mechanical Engineering, Tuskegee University, Tuskegee, AL 36088, USA

³Arctic Technology & Icing Research Group (arcICE), UiT- The Arctic University of Norway

⁴College of Engineering /Department of Biomedical Engineering and Mechanics, Virginia Tech, USA

⁵Department of Mechanical Engineering, University of Eng. and Tech, Peshawar, Pakistan

Received 5 Feb 2025

Accepted 27 Apr 2025

Abstract

This study computationally evaluates the aerodynamic performance of the NACA 65-421 airfoil under disturbed inflow conditions caused by upstream barriers. Simulations were conducted using ANSYS Fluent with the RNG k-ε turbulence model to capture the complex flow characteristics and turbulence effects introduced by enclosing boundaries. The analysis includes detailed contour plots, velocity vector fields, pressure distributions, and velocity profiles at key regions such as the leading edge, trailing edge, and wake zone. Despite the presence of upstream barriers that complicate the inlet flow, the NACA 65-421 airfoil demonstrates satisfactory aerodynamic performance. The leading edge demonstrates significant flow acceleration, contributing to lift generation, while the trailing edge and wake regions exhibit reduced turbulence and rapid velocity recovery, resulting in low drag. Static pressure contours show a stagnation zone at the leading edge and efficient pressure recovery at the trailing edge, supporting favorable aerodynamic characteristics. Under disturbed inflow conditions, the NACA 65-421 airfoil achieves a stable lift coefficient (Cl) of approximately 0.36 and a low drag coefficient (Cd) of about 0.006. Pressure coefficient (Cp) analysis reveals strong suction peaks ($C_p \approx -1.2$) along the upper surface, further enhancing lift-to-drag performance. Numerical results align well with experimental data, validating the airfoil's robustness against inflow disturbances. Overall, the study confirms the NACA 65-421 airfoil's promising aerodynamic properties, highlighting its suitability for a range of applications even under non-ideal inflow conditions.

© 2025 Jordan Journal of Mechanical and Industrial Engineering. All rights reserved

Keywords: NACA 65-421, Airfoil, Obstacles, Aerodynamics, RNG k-ε, CFD, Lift coefficient, Drag coefficient, Pressure coefficient.

1. Introduction

The aerodynamic performance of airfoils under disturbed flow conditions is a critical area of research, particularly in aerospace engineering, wind energy systems, and urban wind turbine applications [1]. Turbulent inflow, often induced by upstream obstacles such as buildings, terrain, or other structures, can significantly alter flow patterns, leading to premature boundary layer separation, increased drag, and reduced lift. Understanding these interactions is essential for optimizing airfoil designs to maintain efficiency in real-world, non-ideal flow conditions.

The NACA (National Advisory Committee for Aeronautics) series of airfoils remains among the most extensively studied due to its versatility across a wide

range of applications, including wind turbine blades and aircraft wings. The NACA 65-421 airfoil, part of the NACA 65-series, is categorized as a laminar flow airfoil specifically designed to minimize drag at moderate Reynolds numbers. This series is particularly effective in low-drag applications. The 65-421, with its relatively thick profile, is especially suitable for wind turbine blades, as it offers efficient lift generation with reduced drag [2].

1.1. Literature Review

The foundational work by Abbott and von Doenhoff on NACA airfoils is among the most frequently referenced in aerodynamic research. They were pioneers in developing performance charts for various NACA profiles and provided detailed explanations of the aerodynamic behavior under different flow conditions. The studies

* Corresponding author e-mail: aalahmer@tuskegee.edu.

elaborated on both laminar and turbulent boundary layer models—critical components in understanding lift and drag generation across a broad range of Reynolds numbers [3].

Computational Fluid Dynamics (CFD) has emerged as a powerful tool for analyzing complex aerodynamic interactions, offering detailed insights into pressure distributions, turbulence effects, and flow separation phenomena [4,5]. In recent years, several studies have explored performance-related aspects of airfoils, particularly for wind energy applications. These investigations often utilize CFD to assess the aerodynamic performance of wind turbine blades at different angles of attack and Reynolds numbers. It has been consistently observed that these two factors significantly influence blade performance, highlighting the importance of designing blades that can adapt effectively to varying wind conditions. For instance, Badran [6] conducted experimental investigations to better understand aerodynamic behavior, focusing on flow separation in two configurations: (a) a high-lift wing with a NACA 4412 airfoil section at elevated angles of attack, and (b) a backward-facing step, analyzing the effects of inlet and outlet flow conditions. Similarly, Juliana et al. [7] performed CFD modeling and simulation of the NACA 4420 airfoil for wind turbine applications. The findings emphasized the necessity of optimizing airfoil geometry to enhance turbine performance, demonstrating that CFD tools are invaluable in understanding and improving aerodynamic efficiency.

Obstacles in the aerodynamic environment frequently induce disturbances such as wake formation, vortex shedding, and boundary layer separation, all of which significantly impact aerodynamic surface performance. These obstacles can originate not only from physical objects like mountains and buildings but also from the inherent variability in wind direction and topography [8]. As such, the interaction between airfoils and nearby obstacles has garnered attention due to its practical relevance in scenarios such as urban wind turbines, low-altitude flights, and rotorcraft operations near buildings and towers [9,10]. Obstacles located upstream of an airfoil can intensify flow turbulence, thereby altering boundary layer development along the airfoil surface. This interaction can affect key aerodynamic parameters, including lift and drag coefficients, and may promote premature flow separation [11,12]. Depending on their size, position, and geometry, nearby obstacles can thus lead to performance degradation by increasing drag and, in some cases, reducing lift [13–15].

A primary effect of placing an airfoil near an obstacle is the early onset of flow separation, which leads to reduced lift and increased drag [16]. This separation occurs when the boundary layer detaches from the airfoil surface due to adverse pressure gradients or turbulence. The resulting wake region, characterized by low pressure, contributes to drag formation [17]. Roshko [18] was among the first in identifying the relationship between vortex shedding and drag, showing that objects within the flow field cause unsteady vortices and fluctuating pressure fields, thereby increasing drag. These findings are particularly relevant when considering passive flow-control devices placed ahead of airfoils, which can amplify

separation and turbulence. The present study supports this, with simulation results showing increased turbulence and separation zones upstream of a NACA 65-421 airfoil. Further exploration into boundary layer separation was carried out by Simpson [19]. The author emphasized that boundary layer separation depends heavily on the location of disturbances and the Reynolds number of the flow.

In this context, CFD has become a vital tool for analyzing complex aerodynamic phenomena that are difficult or expensive to assess experimentally [20]. CFD enables precise evaluation of internal and external flow fields, pressure distributions, and turbulence behavior [21][22]. Versteeg and Malalasekera [23] conducted detailed CFD studies involving airfoil analysis, highlighting the importance of mesh quality and accurate turbulence modeling [6]. In this study, the RNG $k-\epsilon$ turbulence model effectively captured fluid separation and recirculation phenomena around solid obstacles interacting with airfoils. While the Spalart and Allmaras model [24] is widely used in external aerodynamic simulations, this study focused instead on the $k-\epsilon$ models due to their superior capability in capturing the large-scale structures associated with obstacle-induced turbulence.

Turbulence models like the RNG $k-\epsilon$ are critical for accurately representing the complex flow behavior caused by obstacle-induced disturbances, which can significantly influence aerodynamic performance [25,26]. Rao et al. [27] demonstrated that high-fidelity CFD tools improve performance predictions and allow for optimized airfoil designs. Alrawashdeh et al. [28] used COMSOL to model the Magnus Wind Turbine with cylindrical blades, examining stress, torque, and fatigue across different design alternatives. The findings indicated that stress was highest at blade tips and lowest at the base, with implications for turbine performance optimization. Ghenai et al. [29] applied RANS modeling to compare parabolic shrouded wind turbines, showing aerodynamic advantages and improved load management with shrouded configurations. Messaoud et al. [30] investigated sensorless control systems for small-scale vertical axis turbines, emphasizing the importance of advanced control strategies and airfoil design in enhancing turbine efficiency. These studies affirm that proximity to obstacles alters aerodynamic flow in complex and generally detrimental ways, increasing turbulence, flow separation, and vortex shedding. These effects reduce lift and increase drag, underlining the importance of careful analysis in environments involving structural interference with airflow.

Fearn [31] demonstrated the effectiveness of panel methods for airfoil analysis, confirming the potential for accurate aerodynamic assessment and aircraft wing optimization. Nguyen et al. [32] further emphasized the significance of wing geometry in aerodynamic performance, showing that design variations can substantially enhance aircraft efficiency. Sumaryada et al. [33] explored the interaction between Gurney flaps and angles of attack, showing that the addition of flaps improved lift at certain conditions, enhancing airfoil performance. Ackroyd [34] highlighted the historical contributions of Sir George Cayley, whose foundational aerodynamic theories remain relevant today. Devi and Nagaraja [35] numerically analyzed the pitching moment

coefficient of a NACA0012 airfoil across Reynolds numbers ($10^4 < Re < 10^5$) using a novel high-order triangular meshing method with parabolic arcs, demonstrating computational efficiency with linear, quadratic, and cubic elements. The approach reduced computational effort while accurately evaluating this critical aerodynamic parameter affecting airfoil torque. Ravi et al. [36] used CFD to study flow transition around a NACA 4412 airfoil, identifying angles that promote smoother transitions and demonstrating CFD's value in design decision-making. Eleni et al. [37] compared turbulence models for the NACA 0012 airfoil, determining which models best predicted flow separation and distortion. Aminjan et al. [38] investigated wing geometry modification mechanisms, proposing an innovative adaptive wing system using NACA 65-series airfoils (65-212 and 65-2012) with fixed/moving parts controlled by a microcontroller circuit that adjusts curvature in real-time based on CFD-optimized data. Testing demonstrated precise performance with 15.3% and 9% error margins in thickness and position parameters at 0° - 25° attack angles.

1.2. Research Gap, Objectives, and Novelty

Despite extensive studies on airfoil performance under ideal flow conditions, limited research has addressed the aerodynamic behavior of laminar-flow airfoils—specifically the NACA 65-421—under disturbed inflow conditions caused by upstream obstacles. The presence of such obstacles, which introduce turbulence, vortex shedding, and wake interactions, significantly alters the flow field around the airfoil. Previous investigations have primarily focused on clean inflow environments, neglecting practical scenarios where upstream structures or terrain irregularities are common, such as in urban wind energy systems, low-altitude flight, and rotorcraft operations. Moreover, the application and validation of advanced turbulence models like the RNG k - ϵ model in capturing the complexities of such disturbed flow remain underexplored in this context.

The main objectives of this study are:

- To numerically evaluate the aerodynamic performance of the NACA 65-421 airfoil under non-uniform, disturbed inflow conditions caused by upstream cubical obstacles.
- To assess the influence of upstream-induced turbulence and vortex formation on boundary layer development, lift and drag coefficients, and overall aerodynamic stability.

- To employ the RNG k - ϵ turbulence model within ANSYS Fluent to accurately capture complex flow behavior, particularly in regions of high strain rates, separation zones, and wake formation.
- To validate the computational predictions with experimental data, ensuring the reliability of CFD simulations under disturbed inflow scenarios.

This study introduces a novel approach to evaluating the aerodynamic characteristics of a laminar-flow airfoil under realistic disturbed inflow conditions—a scenario that is often overlooked in traditional aerodynamic analyses. The use of the RNG k - ϵ turbulence model enhances the fidelity of the simulations, providing a more accurate representation of the flow structures generated by upstream obstacles. By analyzing detailed flow features such as velocity vectors, pressure distributions, and wake behavior, this work offers new insights into the mechanisms behind lift enhancement and drag mitigation in turbulent environments. Furthermore, the study highlights the robustness of the NACA 65-421 airfoil, confirming its suitability for applications in challenging aerodynamic settings, and provides valuable data to inform future airfoil design and optimization under non-ideal flow conditions.

2. Methodology: Computational Domain and Simulation Setup

Figure 1 illustrates the computational geometry used for the CFD simulation involving the NACA 65-421 airfoil subjected to upstream flow disturbances caused by rectangular obstacles. The simulation domain was configured with a total length of 6 meters and a height of 2 meters, providing ample space for airflow development and minimizing boundary effects on the computed results. The domain was designed to realistically simulate flow interactions while ensuring that external boundaries did not interfere with the internal flow field, maintaining stable and representative computational conditions.

Three square obstacles, each with a thickness of 0.12 meters, were positioned 1.13 meters from the domain's inlet boundary and spaced 0.24 meters apart vertically. The airfoil was strategically placed downstream of the obstacles to study the influence of disturbed inflow conditions on its aerodynamic performance. This arrangement mimics realistic environmental conditions, such as those encountered in administrative aerospace settings where structural interference is common.

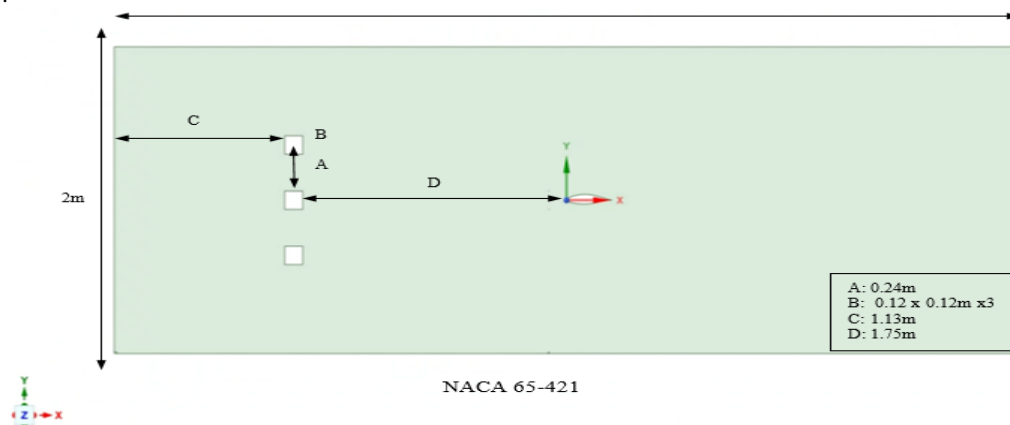


Figure 1. Schematic of the computational domain for NACA 65-421 airfoil with upstream rectangular obstacles

Figure 2 displays the computational mesh, which consisted of a structured quadrilateral grid comprising 321,985 cells, 645,540 faces, and 323,552 nodes. Mesh refinement was applied extensively around the airfoil and the obstacles to accurately resolve boundary layer behavior, flow separation, and vortex formation.

To ensure accurate simulation results while maintaining computational efficiency, a detailed mesh independence analysis was conducted. The mesh employed consisted of 321,985 structured quadrilateral cells, 645,540 faces, and 323,552 nodes. The mesh quality was rigorously monitored, achieving a minimum orthogonal quality of 0.404 and a maximum aspect ratio of 382.81—acceptable values for capturing the complex flow physics, particularly around the airfoil and obstacle regions. As shown in Figure 3, the lift coefficient (C_l) converged to approximately 0.35 when the number of nodes exceeded 323,552, indicating that further mesh refinement had an insignificant effect on aerodynamic predictions. Thus, this mesh configuration was deemed sufficient and used throughout the study. Standard wall functions were also implemented to enhance the accuracy of turbulence modeling near solid boundaries, where boundary layer effects are critical. Additionally, experimental benchmarks were employed to validate the numerical findings, reinforcing the credibility and

robustness of the selected mesh and overall simulation framework.

The simulations were conducted using ANSYS Fluent 23.1, employing a two-dimensional, double-precision, pressure-based solver in transient mode. The RNG $k-\epsilon$ turbulence model was selected due to its robustness and effectiveness in modelling complex turbulent flows encountered in aerodynamic applications. The time-dependent simulation was configured to run for 1000 time steps with a time step size of 0.001 seconds, and a maximum of 20 iterations per time step was used to ensure numerical convergence. Although a separate time step sensitivity analysis was not performed in this study, the chosen time step has been widely adopted in similar CFD simulations and has proven sufficient for maintaining numerical stability and accurately capturing transient aerodynamic behavior under turbulent flow conditions.

Boundary conditions were defined to simulate realistic operating conditions. The inlet was specified with a velocity of 21 m/s and a turbulence intensity of 5%, representing a typical turbulent atmospheric flow. The outlet was set as a pressure-outlet boundary, allowing smooth flow transition out of the domain and minimizing artificial reflection or distortion of the simulated flow.

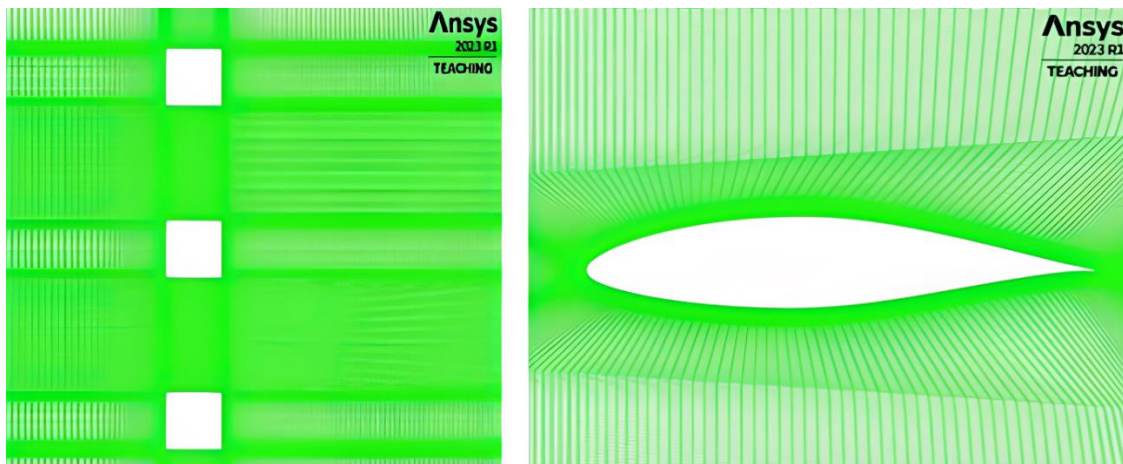


Figure 2. Structured mesh configuration around the airfoil and upstream obstacles

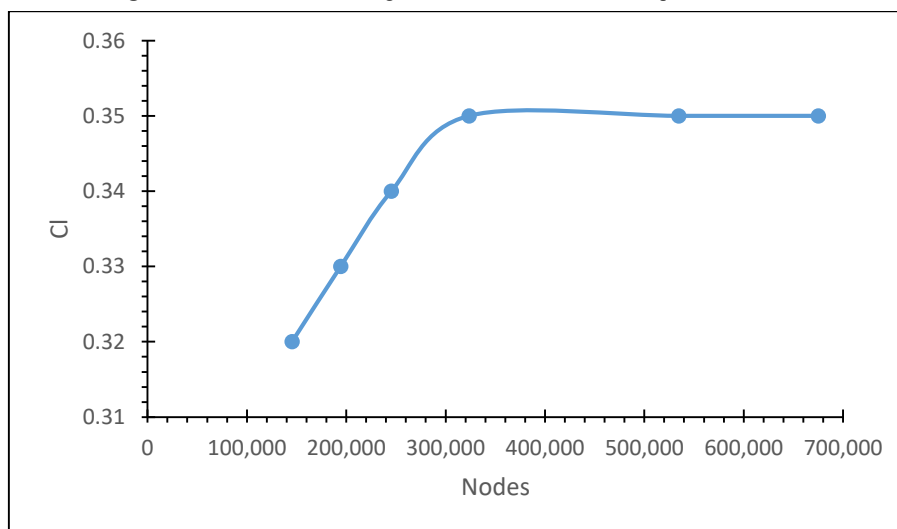


Figure 3. Mesh independence study showing variation of lift coefficient with increasing node count

3. CFD Framework, Numerical Parameters, and Turbulence Modeling

The numerical simulation was conducted in a two-dimensional domain using a transient approach to capture the time-dependent nature of the airflow. A first-order implicit time integration scheme was selected to strike a balance between computational efficiency and acceptable accuracy. The simulation incorporated the RNG k - ϵ turbulence model due to its proven capability in handling complex turbulent flows, especially in scenarios involving flow separation and recirculation around obstacles—conditions commonly encountered in flows interacting with an airfoil and upstream disturbances. To resolve the near-wall behavior accurately, standard wall functions were applied.

Material properties were carefully assigned to both the fluid and solid components within the domain. Air was used as the working fluid, with a density of 1.225 kg/m^3 , specific heat of $1006.43 \text{ J/kg}\cdot\text{K}$, thermal conductivity of $0.0242 \text{ W/m}\cdot\text{K}$, and dynamic viscosity of $1.7894 \times 10^{-5} \text{ kg/m}\cdot\text{s}$. Aluminum was used for the construction of the airfoil and upstream obstacles, with a density of 2719 kg/m^3 , specific heat of $871 \text{ J/kg}\cdot\text{K}$, and thermal conductivity of $202.4 \text{ W/m}\cdot\text{K}$. These properties ensured realistic simulation of both fluid and structural domains.

Boundary conditions were designed to reflect realistic aerodynamic performance [39]. At the inlet, a velocity of 21 m/s was applied in the x -direction, corresponding to a Reynolds number of approximately 3.5×10^5 , with no velocity component in the y -direction. The inlet turbulence was characterized by a turbulent kinetic energy of $1 \text{ m}^2/\text{s}^2$ and a dissipation rate of $1 \text{ m}^2/\text{s}^3$. A pressure outlet condition was imposed at the domain exit, maintaining zero gauge pressure to allow free outflow. All domain walls were modeled as stationary, no-slip surfaces with zero roughness, representing smooth physical boundaries.

To solve the governing equations, a pressure-based solver was employed, which is well-suited for modeling incompressible flows such as those around the NACA 65-421 airfoil [39]. For pressure-velocity coupling, the SIMPLE (Semi-Implicit Method for Pressure-Linked Equations) algorithm was employed due to its robustness and reliability in handling transient simulations, providing a good balance between computational efficiency and solution accuracy. The spatial discretization scheme applied a second-order upwind method for the momentum equations to capture flow gradients more accurately, while first-order upwind schemes were adopted for the turbulent kinetic energy and dissipation rate to promote numerical stability. The simulation was conducted in transient mode with a time step size of 0.001 seconds, totaling 1000 time steps, and each step was constrained to a maximum of 20 iterations to ensure stable convergence and consistent solution progression.

Under-relaxation factors were applied to facilitate numerical stability. The pressure equation was relaxed with a factor of 0.1 , while the momentum equations used a relaxation factor of 0.5 . Turbulent quantities—kinetic energy and dissipation rate—were relaxed using factors of 0.8 . These values were selected to maintain solver stability and ensure convergence without sacrificing accuracy.

Convergence was assessed by monitoring the residuals of the governing equations. Target residual values were set at 1×10^{-5} for continuity, x -velocity, and y -velocity, while turbulent kinetic energy and dissipation rate were targeted

at 1×10^{-6} and 1×10^{-3} , respectively. At the end of the simulation, most residuals had reached or exceeded their target thresholds. The x -velocity residual reached 1.301×10^{-6} , and y -velocity settled at 1.651×10^{-6} . Turbulent kinetic energy and dissipation rate converged to 6.367×10^{-7} and 8.799×10^{-6} , respectively. Although the continuity residual slightly exceeded the target at 1.1485×10^{-4} , the solution was still considered sufficiently converged for aerodynamic analysis purposes.

The RNG k - ϵ turbulence model employed standard constants: $C_\mu=0.09$, $\sigma_k=1.0$, $\sigma_\epsilon=1.3$, $C_1=1.44$, and $C_2=1.92$. These constants are well-established in turbulent flow modeling and provided a reliable framework for predicting flow separation, reattachment, and vortex formation—key phenomena in this study of flow around an airfoil affected by upstream disturbances.

It is worth noting that the RNG k - ϵ turbulence model was chosen for this study due to its enhanced capability to accurately predict complex flow features such as separation, recirculation, and high strain rates—conditions that are particularly relevant in the presence of upstream disturbances affecting the NACA 65-421 airfoil. Unlike the standard k - ϵ model, RNG k - ϵ includes additional terms in the dissipation equation and a modified turbulent viscosity formulation, which improve its performance in flows with strong curvature and swirl. Compared to the Spalart-Allmaras model, which is efficient but primarily suited for attached flows, RNG k - ϵ offers better resolution of turbulent structures in separated or wake regions. While the SST k - ω model provides superior near-wall accuracy, it is more sensitive to freestream conditions and often requires finer mesh and greater computational resources. In contrast, RNG k - ϵ provides a balanced approach with robust and stable convergence behavior, making it a suitable and practical choice for simulating the unsteady aerodynamic behavior of airfoils under disturbed inflow conditions.

4. Results and Discussion

4.1. Flow Characteristics and Velocity Distribution

This study provides a comprehensive analysis of velocity flow fields, pressure distribution, and turbulence characteristics to better understand the aerodynamic behavior surrounding the airfoil. The results below offer insights into the flow dynamics influenced by the upstream obstacles and their interaction with the airfoil.

Figures 4 and 5 illustrate the velocity magnitude contours, providing a visual representation of airflow speed across the computational domain. A significant drop in velocity occurs near the obstacles, accompanied by flow circulations around their top and bottom surfaces—most notably in the leeward regions. This behavior is a result of flow separation, where the high-speed incoming stream interacts with the sharp edges of the obstacles, creating strong recirculation zones [40]. Although the flow gradually recovers downstream, low-velocity regions persist within the wakes, surrounded by turbulent high-velocity zones. These recirculating areas can induce unsteady flow behavior further downstream, particularly in the vicinity of the airfoil.

The flow accelerates around the NACA 65-421 airfoil due to its geometry, with velocity increasing near the leading edge. However, disturbances from the upstream obstacles lead to a non-uniform velocity distribution, potentially affecting the lift and drag forces acting on the

airfoil. Figure 5 also presents X-velocity contours, highlighting the streamwise velocity component. A pronounced reduction in X-velocity appears immediately behind the obstacles, where the flow stagnates, and counter-rotating vortices form due to the obstacle's sharp edges. As the flow continues downstream, X-velocity increases, though the upstream disturbances remain evident and affect the uniformity of the incoming flow—a key factor in determining aerodynamic performance.

Figure 6 presents velocity vector plots, offering insights into both flow magnitude and direction. These vectors reveal complex flow structures, including strong recirculation zones and vortex formation at the leeward sides and surfaces of the obstacles. The wake regions, characterized by low-velocity vortex centers, propagate toward the airfoil and interact with its surface, potentially introducing unsteady aerodynamic forces [41].

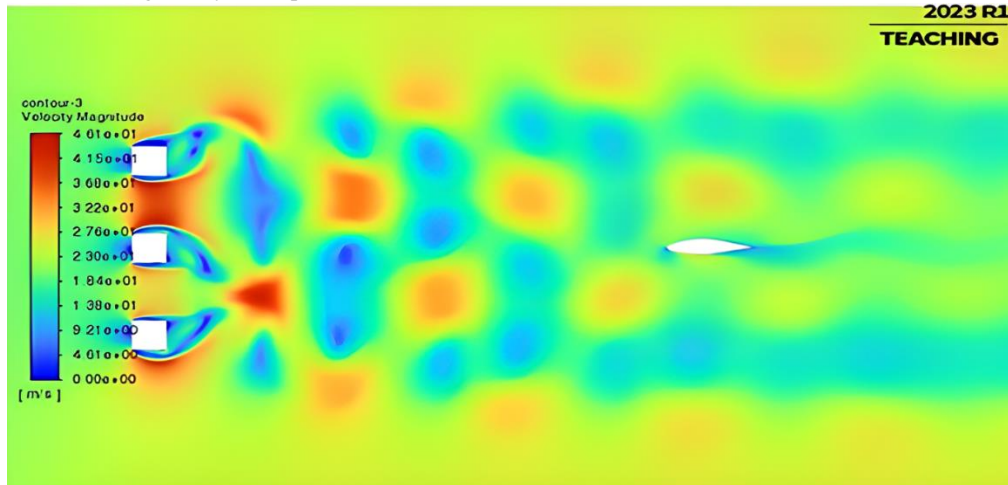


Figure 4. Velocity magnitude contours across the computational domain with obstacles and airfoil

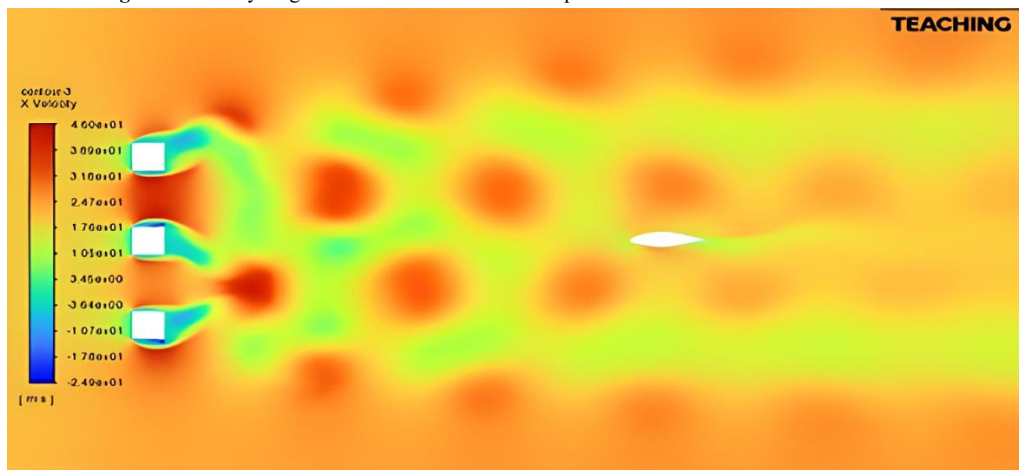


Figure 5. X-Velocity contours in the computational flow domain

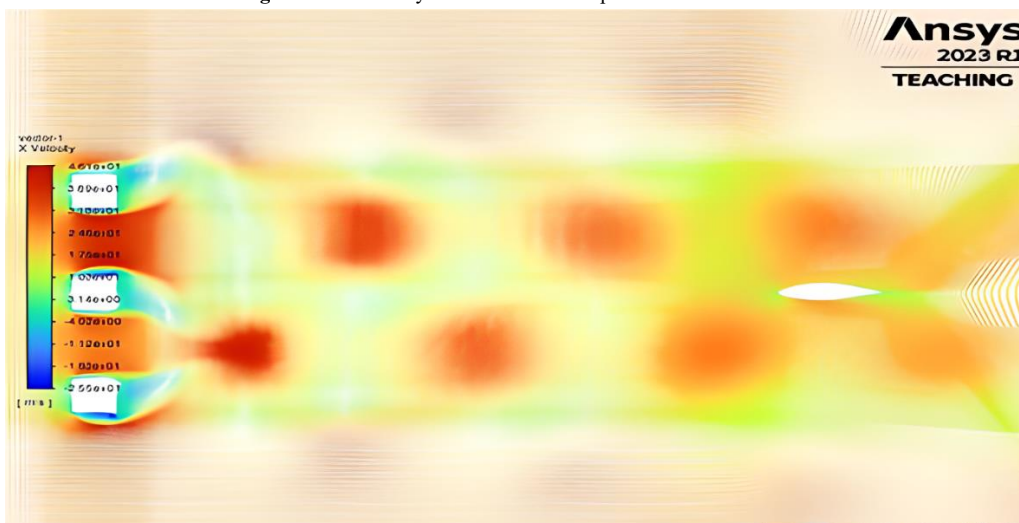


Figure 6. Velocity vector field in the computational flow domain

Figure 7a shows the velocity vectors near the airfoil's leading edge. The vectors indicate an increase in velocity—particularly along the upper surface—as the flow accelerates around the curvature, which is essential for lift generation. However, the upstream-induced disturbances cause localized variations in both direction and magnitude, affecting boundary layer development. In Figure 7b, the trailing edge vectors show how the flow exits the airfoil. Although no flow separation is observed due to the zero angle of attack—mimicking natural conditions in wind turbine blades before pitching—the wake behind the airfoil reflects the influence of upstream-generated vortices, which can impact drag forces.

Figure 7c displays the overall velocity magnitude vectors, affirming that upstream obstacles significantly alter the flow field around the airfoil. The presence of these disturbances leads to increased turbulence, enhanced vortex activity, and non-uniform velocity profiles across the airfoil surface. These effects may alter boundary layer behavior and influence flow attachment near the trailing edges [42]. This comprehensive analysis highlights the importance of accounting for upstream disturbances when evaluating airfoil performance in real-world scenarios, such as wind turbines or aircraft operating near buildings, terrain, or other obstructions.

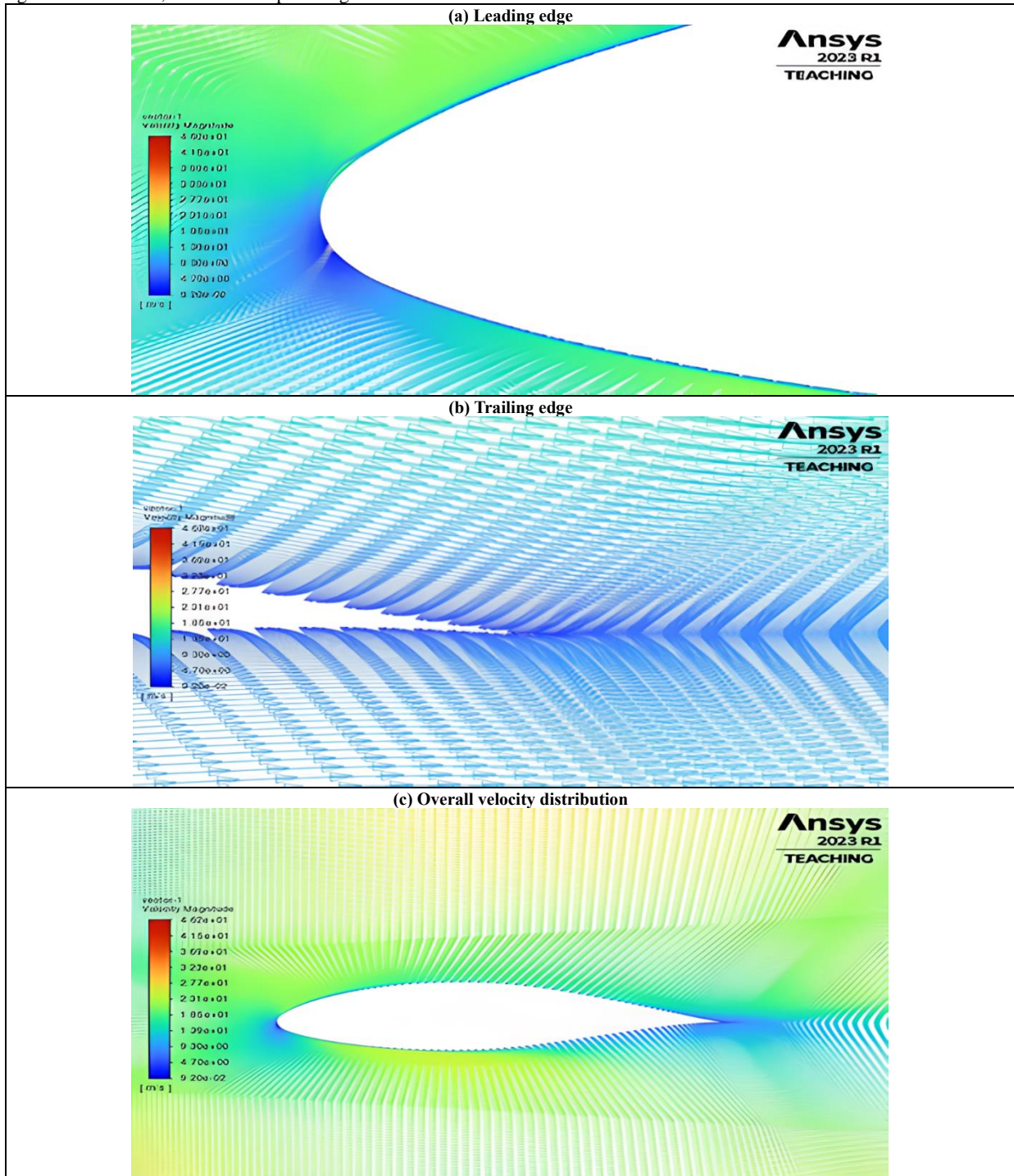


Figure 7. Velocity vector analysis around NACA 65-421 Airfoil: (a) leading edge, (b) trailing edge, and (c) overall velocity distribution

4.2. Velocity Profile Analysis

The velocity profiles at different locations along the NACA 65-421 airfoil, namely the leading edge, mid-edge, trailing edge, and wake region—provide a comprehensive picture of the airflow behavior and its influence on aerodynamic performance. As shown in Figure 8, the velocity increases sharply at the leading edge, rising from approximately 22 m/s to about 25 m/s. This acceleration occurs as the flow transitions from the stagnation point to the suction side (upper surface), reflecting a typical behavior of an efficient airfoil where flow speed increases due to curvature at the front. The rapid acceleration contributes to the formation of a low-pressure zone, which is essential for lift generation [43].

At the mid-section of the airfoil, the velocity remains elevated, with values near 25 m/s. This suggests continued acceleration and indicates that the boundary layer remains attached, with no signs of separation. The smooth and steady rise in the velocity profile reflects favorable aerodynamic conditions, where the attached flow supports consistent lift with minimal disturbance.

Toward the trailing edge, a slight decrease in velocity is observed as the flow begins to decelerate while exiting the airfoil surfaces. The velocity drops to around 22 m/s, yet the flow remains mostly attached, which is beneficial for drag reduction. A short distance downstream from the trailing edge, the wake begins to form. In this region, the flow slows further, dipping below the free-stream velocity (approximately 21 m/s), indicating the presence of a wake with lower-speed flow.

Despite the velocity reduction in the wake, the flow remains relatively stable, with moderate turbulence levels

due to the interaction between the upper and lower boundary layers. The velocity does not fully recover, but the limited extent of turbulence and wake width suggests that the airfoil produces minimal drag while maintaining favorable lift characteristics.

In addition to the velocity profile, pressure recovery plays a crucial role in influencing lift and drag characteristics [13]. A high-pressure region forms at the leading edge due to stagnation, while the upper surface experiences a significant pressure drop as the airflow accelerates, developing the suction effect responsible for generating lift [44]. The resulting pressure difference between the upper and lower surfaces is a primary driver of lift. Toward the trailing edge, pressure recovery, characterized by a gradual pressure rise, helps reduce adverse pressure gradients and support flow continuity along the surface. However, non-uniform inflow caused by upstream obstacles leads to localized pressure disturbances, potentially increasing turbulence and modifying the pressure distribution around the airfoil. These disturbances can slightly reduce aerodynamic performance by increasing form drag and influencing flow separation.

Overall, the shape and progression of the velocity profiles in Figure 8 demonstrate effective flow control around the airfoil. The airflow exhibits steady acceleration at the leading edge, sustained attachment along the mid-chord, and only a slight velocity drop near the trailing edge. The resulting wake shows moderate turbulence with signs of recovery, reinforcing the airfoil's aerodynamic efficiency. These velocity profiles not only confirm good performance but also serve as reliable indicators for detecting potential regions of flow separation, turbulence, and drag.

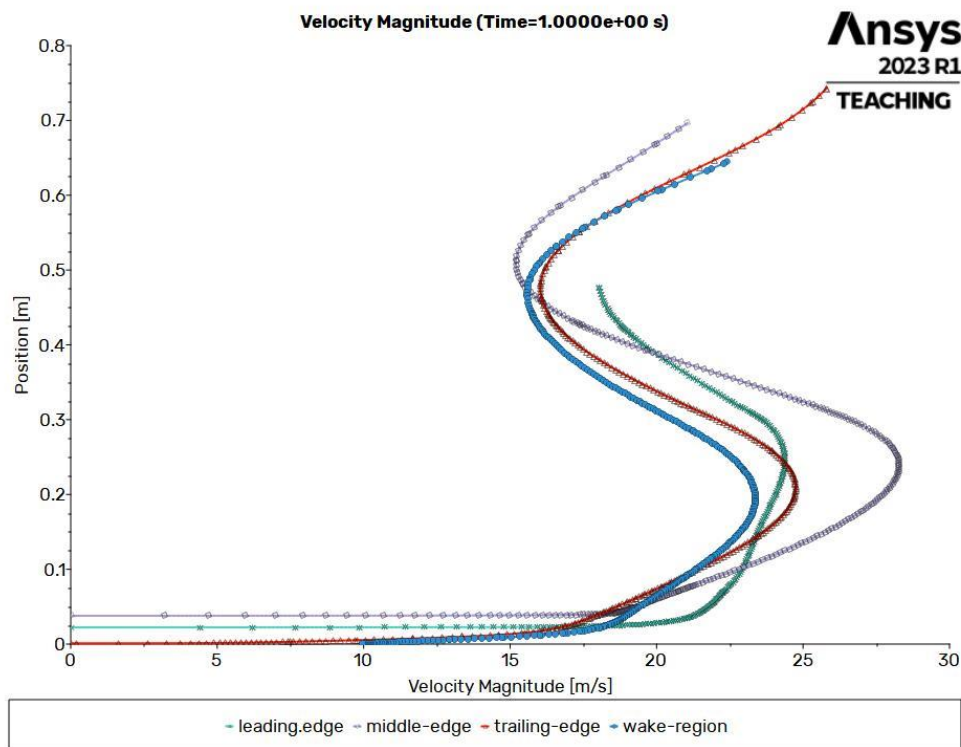


Figure 8. Velocity profiles at different locations along the NACA 65-421 airfoil: leading edge, mid-edge, trailing edge, and wake region

4.3. Static Pressure Distribution

The static pressure contours, illustrated in Figure 9, provide critical insights into the interaction of airflow with upstream obstacles and the NACA 65-421 airfoil. High-pressure zones are observed just upstream of the obstacles, corresponding to stagnation points where the flow decelerates sharply upon encountering sharp edges. This increase in static pressure is a typical response at points of flow impingement. Immediately downstream of the obstacles, static pressure drops significantly, indicating regions of flow separation and recirculation. These low-pressure zones, represented by blue and green areas on the contour map, are characteristic of vortex formation and turbulent wake development.

The alternating bands of low and high pressure in the wake region suggest the occurrence of vortex shedding, where periodic fluctuations in pressure arise due to the continuous formation and detachment of vortices. Such unsteady flow structures can significantly influence downstream components, including the airfoil.

Consistent with airfoil aerodynamics, a high-pressure region is evident at the leading edge of the NACA 65-421 airfoil, marking the stagnation point of incoming flow. As the flow accelerates over the upper (suction) surface, a sharp drop in static pressure is observed, which is essential for generating lift. However, due to the turbulent and non-uniform inflow caused by the upstream obstacles, the pressure distribution along the airfoil becomes distorted [45]. This disturbance introduces localized pressure variations and potentially affects the lift and drag characteristics.

The pressure on the lower (pressure) side of the airfoil remains slightly higher than that on the upper surface, confirming the presence of a favorable pressure differential essential for lift. However, the upstream flow disturbances may compromise the aerodynamic efficiency of the airfoil.

Behind the airfoil, a region of reduced static pressure forms in the wake, consistent with the boundary layers

merging at the trailing edge. The disturbed upstream flow modifies this wake structure, further influencing the airfoil's performance.

In summary, the static pressure contours underscore the significance of upstream obstacles in altering the pressure field around an airfoil. These modifications can lead to increased turbulence, distorted wake patterns, and compromised aerodynamic performance. Therefore, such upstream effects must be carefully considered in practical engineering applications where airfoils operate in disturbed flow environments.

4.4. Pressure Coefficient (C_p) Distribution

Figure 10 presents the pressure coefficient (C_p) distribution over the NACA 65-421 airfoil, providing valuable insight into the pressure contours and overall aerodynamic performance of the airfoil. The C_p distribution is crucial for understanding the pressure variations along the airfoil surface, which in turn influences lift generation and flow behavior [46].

At the leading edge (position = 0), the pressure coefficient reaches its maximum value—indicating the point of highest pressure on the airfoil. This occurs as the airflow stagnates upon impact with the leading edge, resulting in near-zero velocity and a corresponding spike in pressure. This phenomenon is expected due to the formation of stagnation pressure, a characteristic feature of airflow encountering a solid surface head-on.

Following this initial peak, the C_p value drops sharply into negative territory (approximately -1.2), particularly over the upper surface of the airfoil. This rapid decrease corresponds to the acceleration of airflow on the suction side, as per Bernoulli's principle: as fluid velocity increases, pressure decreases. The lowest C_p (most negative value) is observed around 0.02–0.05 m from the leading edge, which marks the region of maximum acceleration and strongest suction. This behavior is typical for high-performance airfoils, where accelerated flow over the curved upper surface helps in creating substantial lift.

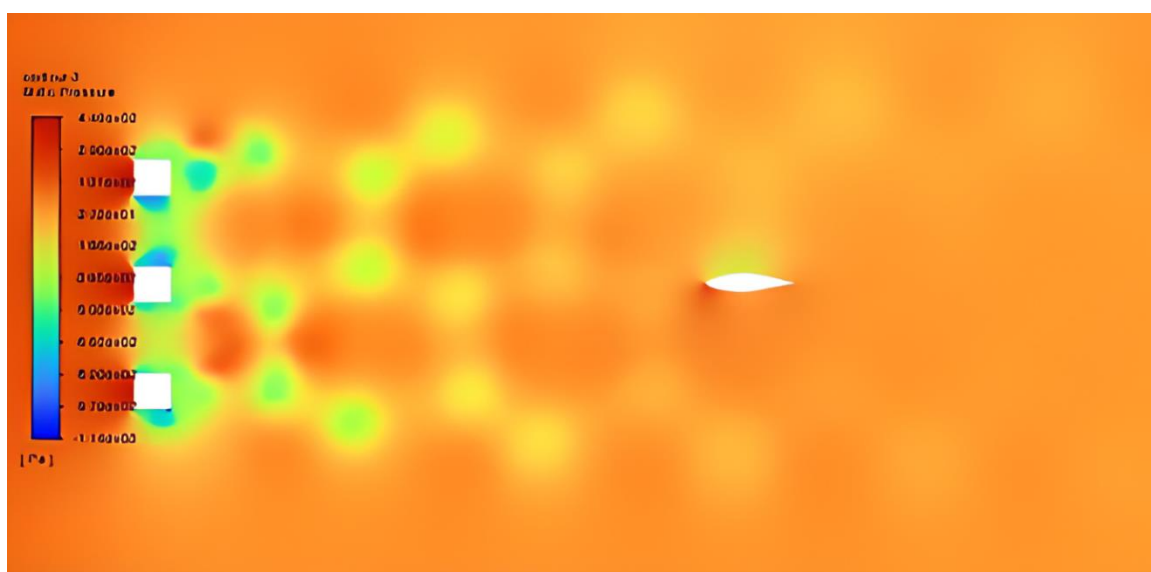


Figure 9. Static pressure contours illustrating the impact of upstream obstacles on the flow behavior and pressure distribution around the NACA 65-421 airfoil.

As the flow continues downstream along the upper surface, the pressure gradually recovers—reflected by a steady increase in C_p values towards zero. This pressure recovery occurs due to the deceleration of the flow as it approaches the trailing edge, especially along the cambered upper surface [47]. Importantly, the absence of sharp changes or abrupt drops in C_p indicates that the flow remains attached to the surface, with no signs of flow separation—an indication of stable and efficient aerodynamic behavior under the given conditions.

This smooth pressure recovery behavior can be further explained by the aerodynamic design of the NACA 65-421 airfoil. Unlike some classical airfoils that may experience a sharp drop in C_p due to sudden flow separation, the NACA 65-421 incorporates a well-optimized camber profile that supports sustained flow attachment over the upper surface. This helps maintain a gradual pressure gradient and prevents abrupt changes in C_p , which contributes to efficient lift generation and reduced drag. Additionally, the disturbed inflow introduced by upstream obstacles may introduce localized pressure fluctuations, particularly near the leading and trailing edges. These fluctuations can attenuate the sharpness of the pressure variations, resulting in a smoother C_p profile. Thus, the combination of the airfoil's geometric characteristics and the influence of upstream disturbances leads to a pressure distribution that is more stable and resistant to flow separation.

On the lower surface of the airfoil, C_p values remain relatively high and steady, ranging between 0.2 and 0.4. These values signify that the flow on the lower side experiences significantly less acceleration and, therefore, maintains higher pressure. Compared to the upper surface,

this creates a pressure differential—higher pressure underneath and lower pressure above—which is the fundamental mechanism of lift generation in airfoils.

The C_p on the lower surface shows minimal variation along the chord, with a slight decrease observed near the trailing edge. This behavior further supports the notion of efficient aerodynamic design, especially in airfoils with optimized camber, where the lower surface plays a passive role in maintaining pressure balance and supporting lift.

At the trailing edge, C_p values from both the upper and lower surfaces converge towards zero. This convergence is essential for smooth flow reattachment and exit, minimizing turbulence and drag at the airfoil's wake.

Under ideal, undisturbed inflow conditions, the C_p profile shown would reflect optimal aerodynamic efficiency. However, in the present case, the airfoil is subjected to disturbed inflow due to upstream obstacles. While the overall pressure distribution remains characteristic of efficient lift generation, the inflow disturbances may introduce localized pressure fluctuations—particularly near the leading and trailing edges—which could impact the net lift and drag performance.

In summary, the C_p distribution in Figure 10 illustrates the typical pressure behavior of a well-performing airfoil. High stagnation pressure at the leading edge, a pronounced suction peak over the upper surface, consistent high pressure on the lower surface, and smooth pressure recovery toward the trailing edge collectively indicate strong lift generation without flow separation. Despite the presence of disturbed inflow, the aerodynamic performance of the NACA 65-421 airfoil remains effective and stable under the simulated conditions.

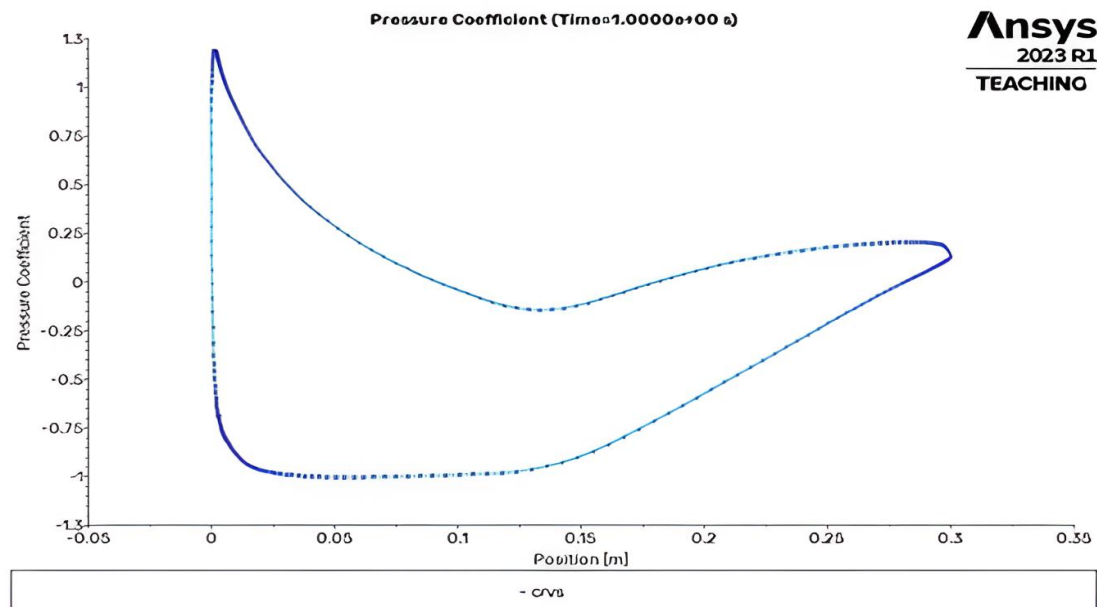


Figure 10. Pressure coefficient (C_p) distribution over the NACA 65-421 airfoil under disturbed inflow conditions

4.4.1. Lift Coefficient (C_l)

The lift coefficient (C_l) plot presented in Figure 11 compares the experimental data [48] with numerical results across multiple time steps, offering valuable insights into the lift performance of the NACA 65-421 airfoil under disturbed inflow conditions. Throughout the simulation, the C_l remains consistently around 0.36, indicating that the airfoil sustains effective lift generation despite the presence of upstream obstructions. This nearly flat temporal C_l curve suggests a quasi-steady aerodynamic state, where the flow structure around the airfoil has stabilized over time.

The close agreement between experimental and numerical results reinforces the credibility of the numerical model, particularly the use of the RNG $k-\epsilon$ turbulence model, the meshing strategy, and the applied boundary conditions. Minor deviations between the two sets of results may stem from uncertainties in the experimental setup—such as wind tunnel discrepancies from real atmospheric conditions—or slight differences in the numerical procedure used to replicate actual operating environments.

The lift coefficient remains largely unaffected by the introduction of new upstream geometries that would typically be expected to alter inflow characteristics. This resilience indicates that the NACA 65-421 airfoil retains its ability to generate lift efficiently even under turbulent inflow conditions caused by upstream disturbances.

In conclusion, the findings confirm the NACA 65-421 airfoil's stable and efficient lift performance despite adverse inflow conditions. This aerodynamic robustness enhances the suitability of the airfoil for applications requiring consistent lift, such as in aviation or wind energy systems, where maintaining stable aerodynamic forces is critical.

4.4.2. Drag Coefficient (C_d)

Figure 12 presents a comparison of experimental and numerical drag coefficient (C_d) results plotted against time steps, illustrating how the drag force on the NACA 65-421 fixed airfoil responds to upstream disturbances.

The figure shows that the drag coefficient exhibits an oscillatory time history, remaining nearly constant and never exceeding 0.006, with the value hovering around $C_d = 0.006$ for most of the time. This stability indicates that the aerodynamic forces on the airfoil are nearly constant and that the airflow around the airfoil has reached an oscillatory, quasi-steady state over time.

The computational drag coefficient results align closely with the experimental measurements, validating the simulation predictions and experimental data [24]. This consistency confirms the accuracy of the simulation configuration, particularly in terms of the turbulence model (RNG $k-\epsilon$), mesh quality, and boundary conditions. The minor discrepancies between the experimental and numerical results may stem from potential sensor inaccuracies, variations in the wind tunnel setup, or deviations in flow conditions assumed to be uniform for both studies.

The relatively low aerodynamic drag coefficient indicates that the NACA 65-421 airfoil is designed for drag reduction, which is characteristic of the NACA 6-series known for its laminar flow properties. This low drag is particularly beneficial in applications where maximizing efficiency is critical, such as in rotating turbine blades or aircraft wings, where minimizing drag is essential to conserve energy and improve performance [49].

The numerical results indicate the clear effects of upstream obstacles on the aerodynamic efficiency of the NACA 65-421 airfoil. While the presence of obstacles changed the pressure distribution, causing a decrease in overall aerodynamic efficiency, the C_d remained relatively stable. The obstacles induced flow separation and vortex formation downstream, leading to pressure fluctuations that negatively impacted lift generation and caused localized drag increases. Despite these disturbances, the overall drag did not exhibit a sharp increase. This can be attributed to the airfoil's efficient design, which maintained a relatively steady flow over the upper surface despite the turbulent inflow. The airfoil's camber and flow attachment were able to reduce some of the drag increase induced by the obstacles, resulting in stable drag values under the tested conditions.

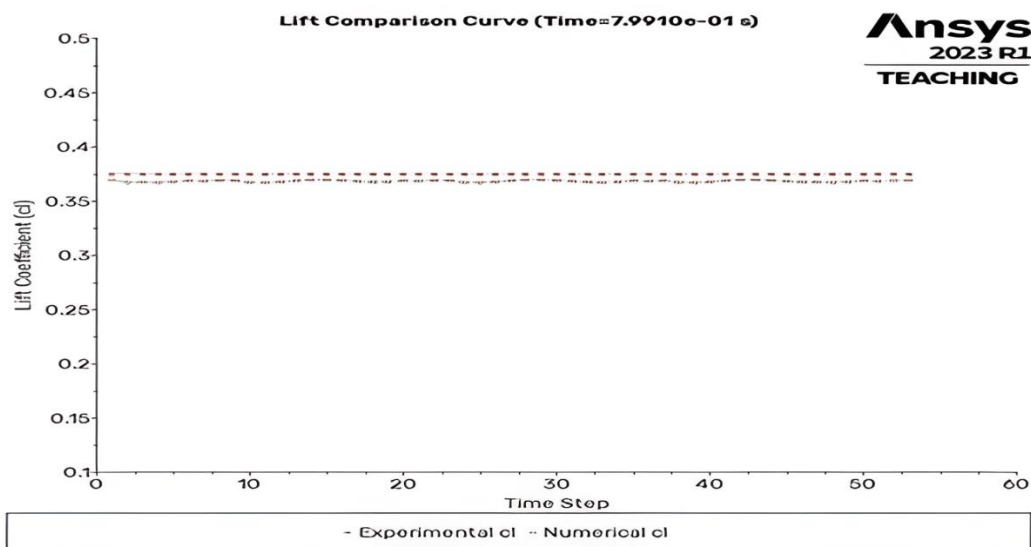


Figure 11. Comparison of Experimental and Numerical Lift Coefficients (C_l) for the NACA 65-421 Airfoil under Disturbed Flow Conditions

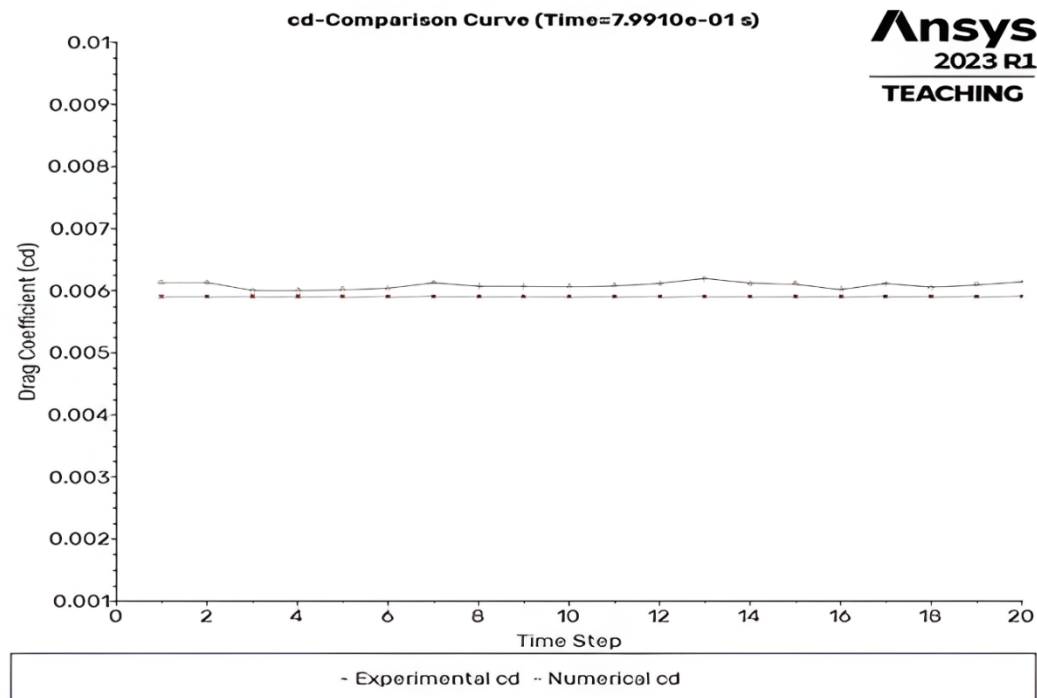


Figure 12. Comparison of Experimental and Numerical Lift Coefficient (Cl) for the NACA 65-421 Airfoil

4.5. Practical Implications

The flow visualizations and contour plots presented in this study, particularly those depicting velocity and pressure distributions around both the obstacles and the NACA 65-421 airfoil, provide valuable insights for real-world aerodynamic design. The identification of separation zones, wake structures, and pressure gradients in turbulent flow regimes holds direct implications for engineering applications involving wind turbine blades and aircraft wings.

In wind turbine blade design, the findings highlight how turbulent interactions influence the boundary layer evolution and surface pressure distribution. For example, regions with high adverse pressure gradients on the suction side can promote early flow separation, leading to reduced lift and increased drag. By understanding these effects, designers can refine blade geometry (e.g., camber, twist, and thickness distribution) to delay separation, enhance the lift-to-drag ratio, and boost energy capture efficiency—especially under variable wind conditions. Likewise, for aircraft wing applications, the detailed pressure and velocity profiles observed around the NACA 65-421 airfoil under turbulent inflow conditions offer critical guidance for improving stall performance and maneuverability. The observed dynamics of flow reattachment and wake oscillation are particularly relevant in low-Reynolds-number flight regimes, such as those encountered by unmanned aerial vehicle (UAVs) and gliders. In such contexts, flow control strategies like vortex generators or boundary layer suction can be employed to stabilize flow and enhance aerodynamic performance.

5. Conclusions

The present study successfully modeled the aerodynamic performance of the NACA 65-421 airfoil under turbulent inflow conditions with an inlet velocity of 21 m/s using the RNG $k-\epsilon$ turbulence model. The findings indicate that the airfoil is highly efficient in producing significant lift ($C_l \approx 0.36$) while maintaining moderate drag ($C_d \approx 0.006$), primarily due to the formation of vortices induced by upstream obstacles. The study also highlighted the importance of considering turbulent inflow conditions when evaluating airfoil performance. The impact of upstream obstacles on the airfoil's aerodynamic efficiency can be summarized numerically as follows:

- The obstacles positioned upstream altered the flow trajectory, contributing to vortex formation downstream. These vortices had a significant impact on both lift and drag by introducing time-dependent side forces. The vortex formation also improved vortex decay and shear at the surfaces of the obstacles, enhancing the flow characteristics.
- Despite the changes in flow caused by the upstream obstacles, the lift coefficient remained relatively high ($C_l \approx 0.36$), indicating efficient lift generation. The drag coefficient remained stable at approximately $C_d \approx 0.006$, reflecting the airfoil's robust design that reduced sharp increases in drag due to turbulence. This stability in C_d suggests that the airfoil's geometry, particularly its camber and flow attachment properties, helped to reduce the adverse effects of the upstream disturbances.
- A close agreement between the experimental and numerical results for the lift and drag coefficients confirmed the accuracy of the CFD simulations. The minor discrepancies between the experimental and numerical results may be attributed to potential

experimental errors or slight variations in the numerical setup, emphasizing the importance of precise modeling.

- The velocity magnitude and vector plots revealed accelerated flow over the upper surface of the airfoil, with no flow separation occurring on either the top or bottom surfaces. The perturbation caused by upstream obstacles created large wake structures and vortices that moved outward behind the obstacles, which affected the overall aerodynamic forces on the airfoil. These vortices contributed to the development of a rich turbulent boundary layer over the airfoil's surface.
- The wake region formed behind the airfoil, characterized by lower velocities, played a key role in the drag experienced by the airfoil. The continuous attached shear layer and the wake structures helped shape the overall drag force, further emphasizing the importance of optimizing airfoil designs for both lift and drag in turbulent environments.

This study highlights the importance of accurately modeling turbulence in aerodynamic simulations, as it has a direct impact on predicting real-world aerodynamic performance. The findings can guide future airfoil designs, particularly in optimizing configurations that balance lift and drag while accounting for turbulent flow conditions.

Further research should investigate the effects of spatial fluctuations at the leading and trailing edges on airfoil performance under irregular flow conditions. This could provide insights into the potential improvements in flow attachment and delay flow separation, which would ultimately enhance aerodynamic efficiency in both wind turbine blades and aircraft wings. By incorporating these insights, future airfoil designs can reduce drag and improve lift performance, especially in scenarios involving turbulent flow induced by upstream obstacles.

Acknowledgment

The authors would like to express their sincere gratitude to the Institute of Industrial Technology, Faculty of Engineering Science & Technology at The Arctic University of Norway (UiT) and Virginia Tech in the United States for providing the opportunity and essential computational facilities to conduct this research. Additionally, the first author would like to thank Al-Balqa Applied University, Faculty of Engineering Technology in Jordan, for granting him a sabbatical leave to work at UiT-The Arctic University of Norway in Narvik.

References

- [1] A. Hossain, P. R. Arora, A. Rahman, A. Z. Jaafar, and A. Iqbal, "Analysis of longitudinal aerodynamic characteristics of an aircraft model with and without winglet," *Jordan Journal of Mechanical and Industrial Engineering*, vol. 2, no. 3, pp. 143–150, 2008.
- [2] Bahador Bakhtiari Nia, Ayat Ghareghani, Saeed Shojae Zadeh, and Vanessa Egan, "Effect of optimal slot location on the performance of cascades of blades," *Proc. Inst. Mech. Eng. Part G*, vol. 235, no. 15, pp. 2208–2224, Mar. 2021, doi: 10.1177/0954410021993698.
- [3] I. H. Abbott and A. E. Von Doenhoff, *Theory of wing sections: including a summary of airfoil data*. Courier Corporation, 2012.
- [4] Y. Taamneh, "CFD simulations of drag and separation flow around ellipsoids," *Jordan Journal of Mechanical and Industrial Engineering*, vol. 5, no. 2, pp. 129–132, 2011.
- [5] H. V Srikanth and M. Kesavan, "Numerical Simulations of Flow and Flame Characteristics of Double Cavity Trapped Vortex Combustor.," *Jordan Journal of Mechanical and Industrial Engineering*, vol. 18, no. 4, pp. 835–845, 2024.
- [6] O. O. Badran and H. H. Bruun, "Experimental Investigation of Turbulent Flow With Separation Over a NACA 4412 Airfoil at Angle of Attack 20 Degree," in *Fluids Engineering Division Summer Meeting*, 2002, pp. 21–28. doi: <https://doi.org/10.1115/FEDSM2002-31067>.
- [7] S. J. Juliyana, J. U. Prakash, K. Karthik, P. Pallavi, and M. Saleem, "Design and analysis of NACA4420 wind turbine aerofoil using CFD," *Int. J. Mech. Eng. Technol.*, vol. 8, no. 6, pp. 403–410, 2017.
- [8] Y. Liu, Y. Shi, A. Aziz, and G. Xu, "Numerical Study on Rotor–Building Coupled Flow Field and Its Influence on Rotor Aerodynamic Performance under an Atmospheric Boundary Layer," 2024. doi: 10.3390/aerospace11070521.
- [9] Q. Zhang, "Interference Suppression Control Method for Aircraft Electromechanical Speed Control System.," *Jordan Journal of Mechanical and Industrial Engineering*, vol. 16, no. 1, pp. 19–29, 2022.
- [10] D. S. Nithya, G. Quaranta, V. Muscarello, and M. Liang, "Review of Wind Flow Modelling in Urban Environments to Support the Development of Urban Air Mobility," 2024. doi: 10.3390/drones8040147.
- [11] J. Klewicki *et al.*, "On the physical structure, modelling and computation-based prediction of two-dimensional, smooth-wall turbulent boundary layers subjected to streamwise pressure gradients," *J. Turbul.*, vol. 25, no. 10–11, pp. 345–368, Nov. 2024, doi: 10.1080/14685248.2024.2392572.
- [12] T. Knopp *et al.*, "Errors and uncertainties in CFD validation for non-equilibrium turbulent boundary layer flows at high Reynolds numbers," *J. Turbul.*, vol. 25, no. 10–11, pp. 399–422, Nov. 2024, doi: 10.1080/14685248.2024.2360195.
- [13] F. Z. Wang, I. L. Animasau, T. Muhammad, and S. S. Okoya, "Recent Advancements in Fluid Dynamics: Drag Reduction, Lift Generation, Computational Fluid Dynamics, Turbulence Modelling, and Multiphase Flow," *Arab. J. Sci. Eng.*, vol. 49, no. 8, pp. 10237–10249, 2024, doi: 10.1007/s13369-024-08945-3.
- [14] E. Lagemann, S. L. Brunton, W. Schröder, and C. Lagemann, "Towards extending the aircraft flight envelope by mitigating transonic airfoil buffet," *Nat. Commun.*, vol. 15, no. 1, p. 5020, 2024, doi: 10.1038/s41467-024-49361-3.
- [15] S. Abdolahi-pour, "Review on flow separation control: effects of excitation frequency and momentum coefficient," *Front. Mech. Eng.*, vol. 10, p. 1380675, 2024, doi: <https://doi.org/10.3389/fmech.2024.1380675>.
- [16] W. Jia and H. Xu, "Effect of synthetic jets actuator parameters on deep reinforcement learning-based flow control performance in a square cylinder," *Phys. Fluids*, vol. 36, no. 8, p. 084113, 2024, doi: <https://doi.org/10.1063/5.0220149>.
- [17] M. Yu, J. T. Hrynuik, D. T. Booth, and N. Poudel, "Freestream turbulence effects on low Reynolds number NACA 0012 airfoil laminar separation bubble and lift generation," *Aerosp. Sci. Technol.*, vol. 149, p. 109145, 2024, doi: <https://doi.org/10.1016/j.ast.2024.109145>.
- [18] A. Roshko, "On the drag and shedding frequency of two-dimensional bluff bodies, NACA Technical Note No. 3169," USA, 1954.
- [19] R. L. Simpson, "Turbulent boundary-layer separation," *Annu. Rev. Fluid Mech.*, vol. 21, no. 1, pp. 205–232, 1989.
- [20] J. Ahn, "Large Eddy Simulation Approaches for Trailing-Edge Heat Transfer in Gas Turbine Blades: A Review," 2025. doi: 10.3390/en18061386.

- [21] B. M. Al-Srayyih *et al.*, "Simulation investigation of the oscillatory motion of two elliptic obstacles located within a quarter-circle cavity filled with Cu-Al₂O₃/water hybrid nanofluid," *Numer. Heat Transf. Part A Appl.*, pp. 1–25, 2023, doi: 10.1080/10407782.2023.2279248.
- [22] S. Y. Ahmed *et al.*, "Investigation of natural convection and entropy generation of non-Newtonian flow in molten polymer-filled odd-shaped cavities using finite difference lattice Boltzmann method," *Numer. Heat Transf. Part B Fundam.*, pp. 1–26, 2024, doi: 10.1080/10407790.2024.2349709.
- [23] H. K. Versteeg, *An introduction to computational fluid dynamics the finite volume method, 2/E*. Pearson Education India, 2007.
- [24] P. Spalart and S. Allmaras, "A one-equation turbulence model for aerodynamic flows," in *30th aerospace sciences meeting and exhibit*, 1992, p. 439.
- [25] M. N. Khalaji, A. Koca, and İ. Kotcioğlu, "Investigation of numerical analysis velocity contours k-ε model of RNG, standard and realizable turbulence for different geometries," *Int. J. Innov. Res. Rev.*, vol. 3, no. 2, pp. 29–34, 2019.
- [26] R. Al-Rbaihat, K. Saleh, R. Malpress, D. Buttsworth, H. Alahmer, and A. Alahmer, "Performance evaluation of supersonic flow for variable geometry radial ejector through CFD models based on DES-turbulence models, GPR machine learning, and MPA optimization," *Int. J. Thermofluids*, vol. 20, p. 100487, 2023, doi: <https://doi.org/10.1016/j.ijft.2023.100487>.
- [27] K. S. Rao, M. A. Chakravarthy, G. S. Babu, and M. Rajesh, "Modeling and simulation of aerofoil element," *Methodology*, vol. 5, no. 02, 2018.
- [28] K. Al bkoor Alrwashdeh, N. S. Gharaibeh, A. A. Alshorman, and M. H. Okour, "Magnus wind turbine effect vertical axis using rotating cylinder blades," *Jordan Journal of Mechanical and Industrial Engineering*, vol. 15, no. 2, pp. 233–443, 2021.
- [29] C. Ghenai, T. Salameh, and I. Janajreh, "Modeling and Simulation of Shrouded Horizontal Axis Wind Turbine Using RANS Method," *Jordan Journal of Mechanical and Industrial Engineering*, vol. 11, no. 4, pp. 235–243, 2017.
- [30] M. Messaoud, B. Hadi, and D. Aissa, "Sensorless control system design of a small size vertical axis wind turbine," *Jordan Journal of Mechanical and Industrial Engineering*, vol. 12, no. 2, pp. 93–98, 2018.
- [31] R. L. Fearn, "Airfoil aerodynamics using panel methods," *Math. J.*, vol. 10, no. 4, p. 15, 2008.
- [32] M. T. Nguyen, N. V. Nguyen, and M. T. Pham, "Aerodynamic analysis of aircraft wing," *VNU J. Sci. Math.*, vol. 31, no. 2, pp. 68–75, 2015.
- [33] T. Sumaryada, A. M. Jaya, and A. Kartono, "Simulating the Aerodynamics Profiles of NACA 4312 Airfoil in Various Incoming Airspeed and Gurney Flap Angle," *Omega J. Fis. dan Pendidik. Fis.*, vol. 4, no. 1, p. 1, 2018.
- [34] J. A. D. Ackroyd, "Sir George Cayley: The invention of the aeroplane near Scarborough at the time of Trafalgar," *J. Aeronaut. Hist.*, vol. 6, pp. 130–181, 2011.
- [35] S. Devi and K. V. Nagaraja, "Investigation of aerodynamic characteristics of NACA0012 airfoil design using parabolic arcs," *Mater. Today Proc.*, vol. 59, pp. 203–207, 2022, doi: <https://doi.org/10.1016/j.matpr.2021.11.085>.
- [36] H. C. Ravi, N. Madhukeshwara, and S. Kumarappa, "Numerical investigation of flow transition for NACA-4412 airfoil using computational fluid dynamics," *Int. J. Innov. Res. Sci. Eng. Technol.*, vol. 2, no. 7, pp. 2778–2785, 2013.
- [37] D. C. Eleni, T. I. Athanasios, and M. P. Dionissios, "Evaluation of the turbulence models for the simulation of the flow over a National Advisory Committee for Aeronautics (NACA) 0012 airfoil," *J. Mech. Eng. Res.*, vol. 4, no. 3, pp. 100–111, 2012.
- [38] K. Khani Aminjan *et al.*, "Numerical and experimental investigation to design a novel morphing airfoil for performance optimization," *Propuls. Power Res.*, vol. 12, no. 1, pp. 83–103, 2023, doi: <https://doi.org/10.1016/j.jprr.2023.02.004>.
- [39] J. Tank, B. F. Klose, G. Jacobs, and G. R. Spedding, "Computer and laboratory studies on the aerodynamics of the NACA 65 (1)-412 at Reynolds number 20 000," in *AIAA scitech 2019 forum*, 2019, p. 2162. doi: <https://doi.org/10.2514/6.2019-2162>.
- [40] Jelena Svorcan, Jonathan M Wang, and Kevin Patrick Griffin, "Current state and future trends in boundary layer control on lifting surfaces," *Adv. Mech. Eng.*, vol. 14, no. 7, p. 16878132221112160, Jul. 2022, doi: 10.1177/16878132221112161.
- [41] P. B. Kirk and A. R. Jones, "Vortex formation on surging aerofoils with application to reverse flow modelling," *J. Fluid Mech.*, vol. 859, pp. 59–88, 2019, doi: DOI: 10.1017/jfm.2018.800.
- [42] N. Thomareis and G. Papadakis, "Effect of trailing edge shape on the separated flow characteristics around an airfoil at low Reynolds number: A numerical study," *Phys. Fluids*, vol. 29, no. 1, p. 14101, Jan. 2017, doi: 10.1063/1.4973811.
- [43] Z.-Y. Li, L.-H. Feng, T. Wang, and Y. Liang, "Lift generation mechanism of the leading-edge vortex for an unsteady plate," *J. Fluid Mech.*, vol. 972, p. A30, 2023, doi: DOI: 10.1017/jfm.2023.569.
- [44] H. Djojodihardjo and N. Thangarajah, "Research, development and recent patents on aerodynamic surface circulation control-A critical review," *Recent Patents Mech. Eng.*, vol. 7, no. 1, pp. 1–37, 2014.
- [45] L. Yan, B. Gao, D. Ni, N. Zhang, and W. Zhou, "Numerical analysis on the system instability of the cavitating flow around hydrofoil induced by the non-uniform inflow," *Int. J. Multiph. Flow*, vol. 152, p. 104074, 2022, doi: <https://doi.org/10.1016/j.ijmultiphaseflow.2022.104074>.
- [46] M. Li, Y. Zhao, Y. Yang, and Q. Zhou, "Aerodynamic lift fluctuations of an airfoil in various turbulent flows," *J. Fluid Mech.*, vol. 947, p. A21, 2022, doi: DOI: 10.1017/jfm.2022.672.
- [47] Z. R. Shu and Q. S. Li, "An experimental investigation of surface pressures in separated and reattaching flows: effects of freestream turbulence and leading edge geometry," *J. Wind Eng. Ind. Aerodyn.*, vol. 165, pp. 58–66, 2017, doi: <https://doi.org/10.1016/j.jweia.2017.03.004>.
- [48] F. Bertagnolio, N. N. Sørensen, J. Johansen, and P. Fuglsang, "Wind turbine airfoil catalogue, Risø National Laboratory, Roskilde, Denmark, August 2001," 2001.
- [49] A. A. Firoozi, F. Hejazi, and A. A. Firoozi, "Advancing Wind Energy Efficiency: A Systematic Review of Aerodynamic Optimization in Wind Turbine Blade Design," 2024. doi: 10.3390/en17122919.